Nuclear Instruments and Methods in Physics Research A 774 (2015) 17–24

Contents lists available at ScienceDirect

Nuclear Instruments and Methods in Physics Research A

journal homepage: www.elsevier.com/locate/nima

The sensitivity of $LaBr_3$:Ce scintillation detectors to low energy neutrons: Measurement and Monte Carlo simulation

J.L. Tain [a,*], J. Agramunt [a], A. Algora [a], A. Aprahamian [b], D. Cano-Ott [c], L.M. Fraile [d], C. Guerrero [e,1], M.D. Jordan [a], H. Mach [b,d,2], T. Martinez [c], E. Mendoza [c], M. Mosconi [f], R. Nolte [f]

[a] Instituto de Física Corpuscular, CSIC–Universidad de Valencia, Apdo. Correos 22085, E-46071 Valencia, Spain
[b] University of Notre Dame, Department of Physics, IN 46556, Notre Dame, USA
[c] Centro de Investigaciones Energéticas Medioambientales y Tecnológicas, E-28040 Madrid, Spain
[d] Universidad Complutense, Grupo de Fisica Nuclear, CEI Moncloa, E-28040 Madrid, Spain
[e] CERN, Geneva, Switzerland
[f] Physikalisch-Technische Bundesanstalt, D-38116 Braunschweig, Germany

ARTICLE INFO

Article history:
Received 18 July 2014
Received in revised form
31 October 2014
Accepted 17 November 2014
Available online 25 November 2014

Keywords:
Neutron sensitivity
Scintillation detectors
Lanthanum bromide
Geant4 simulations
Nuclear data libraries

ABSTRACT

The neutron sensitivity of a cylindrical ⌀1.5 in. × 1.5 in. $LaBr_3$:Ce scintillation detector was measured using quasi-monoenergetic neutron beams in the energy range from 40 keV to 2.5 MeV. In this energy range the detector is sensitive to γ-rays generated in neutron inelastic and capture processes. The experimental energy response was compared with Monte Carlo simulations performed with the Geant4 simulation toolkit using the so-called High Precision Neutron Models. These models rely on relevant information stored in evaluated nuclear data libraries. The performance of the Geant4 Neutron Data Library as well as several standard nuclear data libraries was investigated. In the latter case this was made possible by the use of a conversion tool that allowed the direct use of the data from other libraries in Geant4. Overall it was found that there was good agreement with experiment for some of the neutron data bases like ENDF/B-VII.0 or JENDL-3.3 but not with the others such as ENDF/B-VI.8 or JEFF-3.1.

1. Introduction

Inorganic scintillation detectors find many applications in γ-ray spectroscopy mainly because of the very large detection efficiencies which can be attained. In comparison with high-purity germanium (HPGe) detectors larger intrinsic efficiencies can be obtained because of the larger density and/or effective atomic number. Also in comparison with HPGe detectors, larger solid angle coverage can be reached (close to 4π), because large crystal volumes can be grown and the dead material in multidetector arrangements is more easily minimized. However HPGe detectors offer a much better energy resolution (~ 0.2% at 1 MeV) than scintillation detectors (~ 5% in NaI(Tl), for comparison). The advent [1] of $LaBr_3$:Ce scintillation material, which has about a factor of two better energy resolution compared to NaI(Tl), about 30% larger intrinsic efficiency and much faster scintillation time response, has triggered many new applications. Several properties of $LaBr_3$:Ce used in scintillation detectors have been the subject of thorough investigations as revealed in a search of bibliographic databases. In the present publication we investigate the question of $LaBr_3$:Ce neutron sensitivity to low energy neutrons. Although the results of this study may have other applications we are particularly concerned with the characterization of neutron induced background in the context of nuclear γ-ray spectroscopy applications.

In nuclear research it is often found that the emission of γ-rays, being the primary object of the study, is accompanied (either simultaneously or alternatively) by the emission of neutrons. An example of this situation is the production of neutrons in the reactions used to populate nuclear exited levels in in-beam γ-ray spectroscopy. Another example is the emission of β-delayed neutrons in γ-ray spectroscopy studies of β-decay. Neutrons produced in both cases have in common a relatively low energy (up to a few MeV) and the possibility of inducing background signals through interaction with the γ-ray detector. Therefore a careful investigation of the sensitivity of inorganic scintillation detectors to low energy neutrons is of relevance in these fields.

As an example we take the study of β-decay using the total absorption γ-ray spectroscopy (TAGS) technique [2]. The technique aims to determine accurately the β-intensity distribution for complex decays using a high efficiency 4π scintillation detector.

* Corresponding author. Tel.: +34 963543497; fax: +34 963543488.
E-mail address: tain@ific.uv.es (J.L. Tain).
[1] Present address: Universidad de Sevilla, Departamento FAMN, E-41012 Sevilla, Spain.
[2] Present address: National Centre for Nuclear Research, Division BP1, PL-00691 Warsaw, Poland.

0168-9002/$ - see front matter © 2014 CERN for the benefit of the Authors. Published by Elsevier B.V. This is an open access article under the CC BY license (http://creativecommons.org/licenses/by/4.0/).
http://dx.doi.org/10.1016/j.nima.2014.11.060

The intensity is obtained from the total absorption spectrum by deconvolution with the appropriate response. In the study of β-decay of neutron-rich nuclei one encounters the phenomenon of β-delayed neutron emission in nuclei away from the valley of β-stability. If the decay proceeds to levels above the neutron separation energy in the daughter nucleus the emission of neutrons competes efficiently with γ-ray de-excitation. The emitted neutron can interact with the detector introducing effects in the spectra which must be subtracted if we are to obtain the correct information from the analysis of the data. The quantification of this contamination has been the primary motivation for a research programme looking at several inorganic scintillation crystals, using both Monte Carlo (MC) simulations and measurements. In the present publication we report on the studies performed for the case of $LaBr_3$:Ce material that has been considered for the construction of a new spectrometer in the DEcay SPECtroscopy (DESPEC) experiment [3] at the Facility for Antiproton and Ion Research (FAIR).

Neutrons interact with matter in a complex way through a series of processes whose probability varies strongly depending on isotope and neutron energy. The neutron sensitivity of a scintillation detector, or probability of detecting an incoming neutron, and the associated energy response are influenced by all intervening materials and their geometrical disposition. The experimental determination of the neutron sensitivity requires measurements with the actual detector at the neutron energies of relevance, which is difficult to do. The use of MC simulations for the estimation of this quantity is very appealing because of its generality. However, it is not obvious that MC codes available on the market can provide the detector response with enough accuracy to be useful. In this work we investigate experimentally the response of a $LaBr_3$:Ce detector to neutrons at several energies below 2.5 MeV and compare them with MC simulations. This study is performed with well characterized pure neutron beams as a necessary step towards the application to more complex mixed neutron-gamma fields encountered in spectroscopy experiments.

2. Neutron interactions

Low energy neutrons interact with matter through a series of processes whose importance, as quantified by the cross-section, depends strongly on the neutron energy and the isotopic composition. The main processes contributing to the total neutron cross-section below few MeV for non-fissile isotopes are elastic and inelastic scattering and radiative capture. The questions considered below, exemplified by the case of $LaBr_3$:Ce, apply to inorganic scintillation materials in general.

Fig. 1 shows the macroscopic group cross-sections for $LaBr_3$:Ce(5%) for the three processes that exhaust the total cross-section in the energy range from 1 keV to 10 MeV. The group cross-sections are obtained with the code PREPRO [4] from the ENDF/B-VII.0 [5] evaluated nuclear data file. Group cross-sections represent averages over neutron energy intervals (shown in the figure). They take into account the neutron cross-sections for all the stable isotopes of the three relevant elements Br, La, and Ce. As observed the elastic process dominates in the whole energy range, the inelastic channel grows rapidly above the threshold related to the lowest excited state, and the capture channel decreases strongly with energy.

The elastic scattering process generates signals in the scintillation crystal through the energy loss of recoiling nuclei. Given the large masses of the target nuclei, the recoil energies are small (a maximum of 0.25 MeV for the collision of a 5 MeV neutron with ^{79}Br). In addition, due to the large ionization density produced by the low energy heavy recoil, the light output of the scintillation crystal will be strongly quenched with respect to the light output produced by electrons (γ-rays). This is a well known phenomenon in scintillation materials. In the case of $LaBr_3$:Ce a quenching factor larger than 2 has been observed [6] for α particles and even stronger quenching can be expected for heavier particles [7]. As a consequence the recoiling nuclei will give a negligible signal, below practical detection thresholds, for neutrons up to several MeV and are of no concern for our purposes.

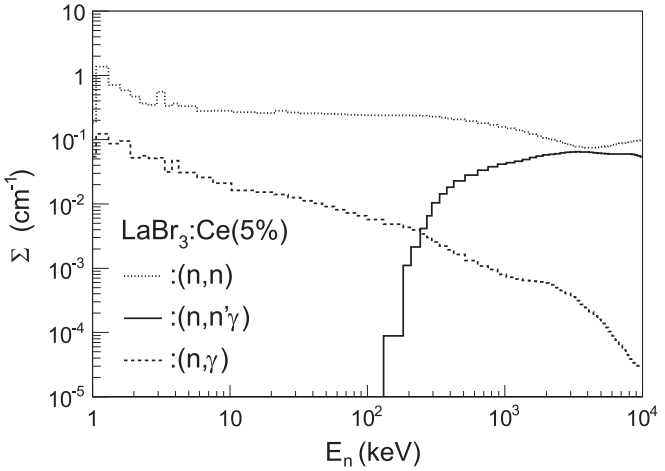

Fig. 1. $LaBr_3$:Ce(5%) group cross-sections for elastic, inelastic and radiative capture neutron reaction channels.

In the case of inelastic and radiative capture reactions γ-rays are generated as secondary particles. They can easily produce a detectable signal indistinguishable from the primary radiation of interest, making these channels the biggest concern in γ-ray spectroscopy. Considering the cross-section dependence with neutron energy (see Fig. 1), one expects that the inelastic channel dominates except below the threshold (few hundred keV). The energy release is limited by the neutron energy in the case of inelastic reactions, while in the case of capture reactions it is equal to the neutron separation energy (typically ranging from 5 to 10 MeV) plus the neutron energy. Because of this, the contamination coming from inelastic scattering concentrates at low energies in the spectrum while that coming from capture shows up at high energies. In addition, due to the nuclear level density variation with excitation energy, the inelastic channel is associated with the emission of a few γ-rays mostly of well known energy, while the capture channel is associated with an electromagnetic cascade of average multiplicity $m = 4$–5 and unknown energy distribution, including high energy primary γ-rays. How this radiation deposits energy in a given detector depends on its geometry. Therefore the measured neutron sensitivity and spectral distribution is specific to a given set-up. For example, the capture process will produce a continuum distribution in small detectors while high energy peaks corresponding to the full absorption of the cascade will appear for large volume detectors [8].

Modern general purpose MC simulation codes for the transport and interaction of radiation in matter have reached a high degree of predictive power in the case of electromagnetic interactions. In order to be applied to the calculation of the sensitivity of γ-ray spectrometers to low energy neutrons, a MC code must include a proper description of the neutron transport and reaction final state. This description should be based on the information contained in evaluated databases for reaction cross-sections, angular distributions, etc., as well as on the information available in nuclear structure databases for excited level schemes and de-excitation patterns.

3. Experiment

In order to investigate the neutron sensitivity of $LaBr_3$:Ce material a small detector was irradiated with neutron beams of well defined energy spanning the energy region from 40 keV (pure radiative capture) to 2.5 MeV (dominated by inelastic scattering).

The detector consists of a cylindrical ⊘ 1.5 in. × 1.5 in. crystal module (Brillance 380, from Saint-Gobain [9]) coupled to a Photonis XP20D0/B Photomultiplier Tube (PMT) with a VD184K/T voltage divider. The module's canning, made of aluminium, has a thickness of 0.5 mm. The crystal is wrapped in a thin layer of reflecting material (type and thickness not provided by the manufacturer). Between crystal and canning there is a layer of shock-damping material also of unknown composition. The total thickness of this material is ~1.2 mm at the sides and ~1.9 mm at the front. The optical window is made of borosilicate glass and has a thickness of 5 mm. No information was available on the exact Ce doping concentration of the crystal, although 5% is the standard value supplied by the manufacturer.

3.1. Measurements

The measurements were carried out in 2009 at the 3.75 MV Van de Graaff Accelerator of the Physikalisch-Technische Bundesanstalt (PTB) in Braunschweig [10]. A low-scatter hall is available for the production of monoenergetic neutron reference fields in open geometry. The amount of room-return neutrons scattered from the concrete walls or from the support structures is reduced as much as possible by the large dimensions of the hall (footprint: 24 m × 30 m, height: 14 m), a low-mass grid floor 6.25 m above the ground floor and by using low-mass constructions for mounting neutron production targets, detectors and ancillary equipment. In addition care was taken to position the potential scattering elements in the experimental setup (see Fig. 2) at a distance from the detector sufficient to ensure that the solid angle fraction subtended is below 0.1%. The remaining fraction of stray neutrons was measured using the shadow cone technique or discriminated by time-of-flight measurements as is explained below.

Up to five different quasi-monoenergetic neutron energy beams were produced using the proton beam of the accelerator and two different reactions: ^{7}Li(p,n)^{7}Be and ^{3}H(p,n)^{3}He. Table 1 shows the combination of target, proton energy and detector position (see Fig. 2) used for each energy. The table also gives the calculated average neutron energy [11] and the estimated neutron fluence for a nominal beam intensity of $I_p = 1$ μA. On average, actual beam intensities ranged from 1 to 2 μA.

The proton beam is pulsed with a frequency of 1.25 MHz allowing the measurement of neutron Time-of-Flight (ToF). From the ToF information it is possible to reconstruct the actual neutron energy distribution and discriminate time-uncorrelated background events.

The signals from the voltage divider are processed to give time and energy information. The signal from the 8th dynode is processed using a preamplifier (Tennelec 245) and a spectroscopic amplifier (Ortec 671) to obtain the deposited energy signal. The anode signal is processed using a timing filter amplifier (Ortec 474) and a constant fraction discriminator (Ortec 583B) to obtain the timing signal. The timing signal starts a Time-to-Amplitude Converter (TAC) unit (Ortec 567), which is stopped by the proton beam pickup signal, providing the ToF measurement. A second TAC unit is started by a 100 Hz precise clock signal, providing the system dead time. The TAC and amplifier signals are sent to the Ortec 8k A413 Amplitude to Digital Converter (ADC) of the Gasific CAMAC/FERA Data Acquisition (DAQ) system [12]. The data are registered event by event in list-mode on a computer disk. The neutron beam intensity is obtained from the counts registered along the run in a De Pangher long counter (PLC) [13] at 98° and a second long counter designated New Monitor (NM) at 17°. Both monitors were calibrated in dedicated runs for each proton beam energy and target combination, using primary reference instruments. For neutron energies below 2 MeV, a recoil proton proportional counter filled either with a mixture of H_2 (96.5 vol.%) and CH_4 (3.5 vol.%) or with C_3H_8 is used. Above 2 MeV a recoil proton telescope is employed.

In order to identify and subtract background signals better from the energy spectrum a shadow cone was placed between the neutron production target and the detector (see Fig. 2) during roughly half of the total irradiation time. In this way two measurements were carried out for every neutron energy. With the shadow cone the crystal registers the indirect radiation coming from neutron interactions in the surrounding materials including the PMT, detector support structure, and the walls of the experimental hall. The shadow cone has the shape of a truncated cone (small diameter 28 mm, large diameter 69 mm) and consists of 20 cm of Fe followed by 30 cm of Polyethylene. The position of the cone was adjusted to minimize the amount of surrounding material shielded.

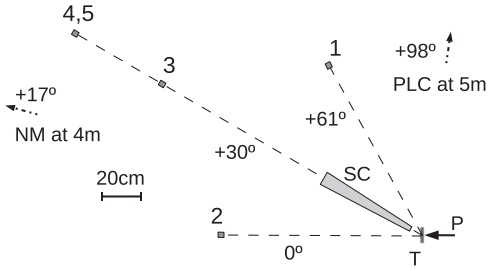

Fig. 2. Schematic layout of the experimental setup. P: proton beam, T: Target, SC: shadow cone, 1–5: detector positions. The number indicates order in Table 1. PLC and NM neutron monitors are outside the figure in the direction and distance indicated. See text for further details.

Table 1
Target composition, proton beam energy E_p, detector distance d and angle θ, nominal neutron energy E_n and neutron fluence Φ_n.

Target	E_p (keV)	d (cm)	θ (deg)	E_n (keV)	Φ_n (sr^{-1} s^{-1} μA^{-1})
LiF	1937	100	61	45	2.48×10^5
	1937	100	0	139	7.02×10^5
	2297	150	30	516	1.17×10^6
^{3}H/Ti	2047	200	30	1058	4.15×10^6
	3353	200	30	2242	1.39×10^7

3.2. Analysis and results

The detector energy calibration is obtained from measurements with standard sources (^{22}Na, ^{60}Co, ^{137}Cs, and Am/Be), and from

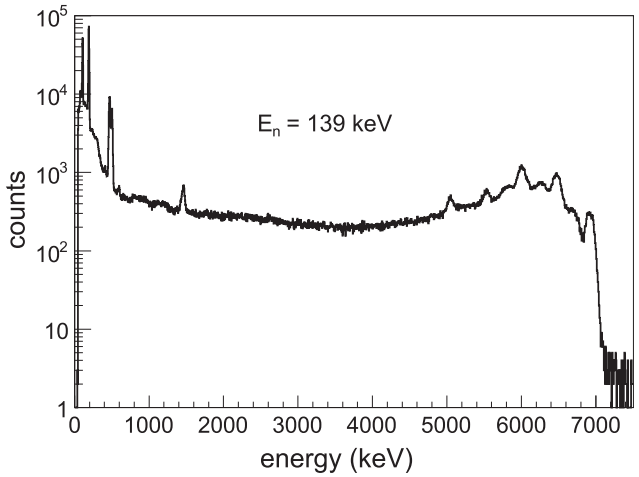

Fig. 3. Energy spectrum measured in the detector at the nominal neutron energy $E_n = 139$ keV.

contaminant peaks coming both from natural radiation and from γ-rays produced in the LiF production target. Fig. 3 shows the spectrum of energy deposited in the measurement at 139 keV nominal neutron energy where no inelastic peaks are expected. It is possible to identify peaks coming from ^{7}Li(p,p′): 478 keV, ^{19}F(p,p′): 110 and 197 keV, and ^{19}F(p,α): 6.13, 6.92 and 7.12 MeV, as well as the annihilation radiation peak (511 keV), the ^{40}K peak (1460 keV) and the 1436 keV intrinsic contamination line from ^{138}La decay. The energy calibration curve shows a strong non-linearity in spite of the use of a voltage divider optimized to maintain the linearity and running the PMT at a relatively low supply voltage of −900 V. This is a well known effect that is due to the high light yield and short scintillation time of $LaBr_3$:Ce which enhances the non-linear behavior of the PMT with increasing dynode current. Because of this effect the energy range up to 10 MeV is divided into three intervals, each with a different calibration function. The lower threshold in the energy spectra is found to be $E_{th} = 50$ keV. The detector resolution calibration is determined from the same data. The energy dependence of the full width at half maximum (FWHM) of the Gaussian peaks is described by the relation $FWHM = 1.033E^{0.4677}$, when the energies are expressed in keV. To calibrate the TAC an Ortec 462 Time Calibrator was used giving a value of 0.244 ns per ADC channel.

The list-mode data were converted into ROOT Trees [14] for the off-line analysis. Two-dimensional spectra of deposited energy versus ToF were constructed and used to unambiguously identify neutron-induced signals from the ToF gated projections. As an example we show in Fig. 4 the ToF spectrum for the measurement at a nominal neutron energy of 1058 keV both with (WSC) and without (NSC) the shadow cone. The WSC spectrum is arbitrarily normalized and is associated with background signals. The normalization of the WSC spectrum is adjusted to reproduce the NSC ToF spectrum in the vicinity of the neutron peak. In the NSC spectrum one can identify the prompt peak (P) at time t=700 ns associated with the interaction of the electromagnetic radiation produced by the proton beam on the target. The prompt peak provides the reference for the ToF determination. The peak (N) visible at t=564 ns corresponds to neutron beam interactions. A small satellite peak (S) can also be observed at t=592 ns. The satellite peak S contains about 10% of the counts in the neutron peak N and has a similar deposited energy spectrum (same peak structure). The origin of the satellite peak is uncertain. However, it cannot originate from neutrons scattered in the setup since the apparent ToF is 20 ns shorter (notice that time runs backwards in the figure) than for the fastest neutrons produced in the reaction (at 0°) if they arrived directly to the detector. We believe that the peak is an artifact of the electronics.

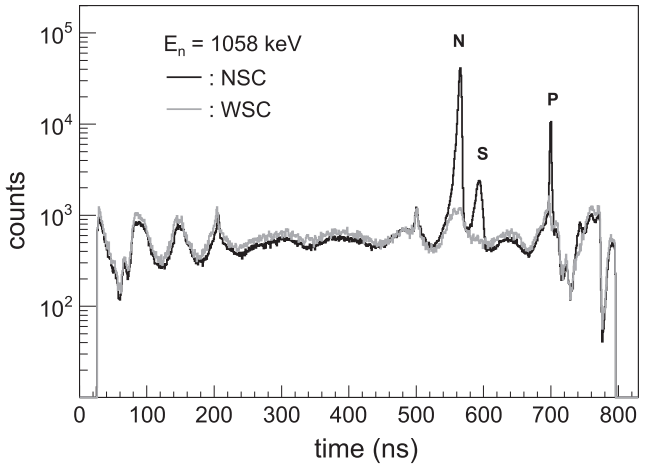

Fig. 4. ToF spectrum obtained at the nominal energy $E_n = 1058$ keV with (WSC) and without (NSC) shadow cone. The WSC spectrum is arbitrarily normalized (see text). P: prompt peak, N: neutron peak, S: satellite peak.

Table 2 gives the limits of the ToF region identified in each case as being due to neutron interactions, converted to the equivalent neutron energy interval. Also given are the centroid ($\overline{E}_n$) and root mean square (*rms*) values of the corresponding neutron energy distribution. We should note that this experimental energy distribution is used as input for the MC simulations. In Table 2 we also give the number of incident neutrons N_n for each case. This number was calculated by integrating the neutron fluence Φ_n over the solid angle subtended by the crystal. The neutron fluence was obtained by averaging the result of both PLC and NM neutron monitors. The values obtained from both monitors agree within better than 1% except for the measurements at $\overline{E}_n = 128$ keV and $\overline{E}_n = 507$ keV where it was 2.5% and 7.4% respectively. The monitor calibration run provides the neutron fluence at the reference angle $\theta = 0°$. The conversion of this number to the value at the angle where the detector was effectively placed was done with the help of the program EnergySet [11]. The uncertainty in the value of N_n given in Table 2 includes the monitor calibration uncertainties. In the case of the measurement at the highest energy there were doubts about the correct positioning of the detector. This was corroborated later in the ToF analysis. On the other hand it is clear that the measured centroid of the ToF distribution (Table 2) reproduces rather well the calculated value of the energy (Table 1) in the remaining cases. Therefore we used the calculated value $E_n = 2242$ keV to make an estimate of the correction (−5%) needed to the nominal distance of 200 cm for this measurement. This corresponds to a 10% increase in the solid angle which was adopted. At the same time a 10% systematic uncertainty was added to the calculated number of neutrons given in Table 2.

The number of counts in the detector due to neutron interactions N_c can be obtained from the integration of clean neutron-induced energy spectra. Clean spectra were obtained by subtracting the normalized WSC spectra from the NSC spectra. In both cases the deposited energy spectra were obtained gating the two-dimensional spectra over the appropriate ToF interval. This procedure cannot be applied for the measurements at $\overline{E}_n = 42$ keV and $\overline{E}_n = 128$ keV because the corresponding WSC measurements are lacking. At both of these energies we restrict the comparison with the MC simulation to the range of deposited energies above 1.6 MeV, which is free from contamination. This limit is coming from the energy spectra obtained by applying ToF gates on both sides of the neutron peak, which show a negligible number of counts beyond 1.6 MeV. The number of counts N_c and the corresponding limits of integration of the energy signal are given in Table 3. The values are corrected by the DAQ system dead time, which was always below 12%. The quoted uncertainty also reflects (when appropriate) the uncertainty on the background (WSC) normalization factor. The neutron sensitivity ε_n was obtained dividing N_c by the number of neutrons impinging on the detector N_n, $\varepsilon_n = N_c/N_n$. The experimental neutron sensitivity ε_n^{exp} calculated in this way is given in Table 3. The deposited energy spectra normalized to the number of counts and corrected for dead time are compared with the corresponding simulated ones in the following section.

Table 2
Measured neutron beam energy range, mean energy $\overline{E}_n$ and *rms* value of the neutron energy distribution, and the number of incident neutrons N_n.

E_n range (keV)	$\overline{E}_n$ (keV)	*rms*	N_n (keV)
34–50	42.2	3.9	$7.41(14) \times 10^5$
108–143	128.3	6.8	$3.16(7) \times 10^6$
439–546	506.8	17.1	$2.29(9) \times 10^6$
841–1136	1031.4	45.7	$4.52(7) \times 10^6$
1839–2501	2242	123.2	$8.8(9) \times 10^6$

4. Monte Carlo simulations

The Geant4 simulation toolkit [15] was chosen to calculate the detector response to neutron interactions. Geant4 is suited to this purpose since it includes the so-called High Precision Neutron Models which allow the detailed simulation of the relevant neutron interactions (elastic collisions, inelastic interactions and radiative capture) below 20 MeV. The necessary information about cross-sections, angular distributions and final states is retrieved from the G4NDL neutron data library. This library, provided together with the simulation package, is based on standard evaluated neutron databases.

Historically a number of independent evaluated neutron data libraries have been developed over the years based on the steadily increasing body of experimental information. The most widely used databases are ENDF/B [5], JENDL [16], JEFF [17], BROND [18] and CENDL [19]. In the different libraries the range of isotopes included and the associated information vary. In addition the different evaluations differ, sometimes by large amounts, for given quantities. The evaluation work is a dynamic process, with the different libraries being updated every certain time. Thus it is clear that, when simulating neutron processes, it is very important to be able to compare the results from the use of different libraries. This option is not included in the standard distribution of Geant4 which uses the G4NDL library written in a special data format. In view of this situation a software tool has been developed at CIEMAT [20] to transform any evaluated neutron data library written in the standard ENDF-6 data format into the G4NDL data format and thus allow intercomparisons. The data for a number of libraries can be obtained in "ready to use" format on-line [20].

As was mentioned earlier another important requirement for a reliable simulation is the correct description of the final state after the neutron reaction. In the present study the description of the γ-ray emission is particularly important. In the case of inelastic scattering, Geant4 uses the information in nuclear databases to generate the associated electromagnetic radiation. This information comes from experimental level schemes and is more or less complete depending on the isotope, but in general deteriorates rapidly with excitation energy. In the case of capture, the information in nuclear databases is even more scarce. Moreover this information is often stored in the form of photon intensities and/or multiplicities which do not permit the generation of cascades conserving the energy (the sum of the energies of the emitted γ-rays should equal the excitation energy of the capture state). This point is critical in the simulation of large 4 $\pi\gamma$-ray detectors which can absorb the full cascade energy. Therefore we have implemented a new C++ class that generates realistic γ-ray cascades and is called, instead of the standard Geant4 class G4NeutronHPCapture, whenever the neutron undergoes a radiative capture process. The MC generation of cascades in the new C++ classes uses the Nuclear Statistical Model (NSM). The statistical model of the nucleus (see for example Appendix A of Reference [21]) provides a parametrized description of the energy variation of level densities for given spin-parity and of photon strength functions for given electromagnetic character and multipolarity. From a knowledge of the ground state spin-parity for the target isotopes and assuming s-wave capture, capture cascades can be generated. The NSM model implemented in the present case is a simplification of the model described in Ref. [21], in the sense that it does not use the experimentally known level scheme at low excitation energies in the final nucleus. Therefore this cascade generator is not able to reproduce the emission of specific γ-rays. However, it is able to provide cascades with the correct total energy and realistic γ-ray multiplicities and energy distributions.

Table 3
Mean energy of neutrons $\overline{E}_n$, signal energy range, number of counts N_c in this energy range, the corresponding experimental neutron sensitivity ϵ_n^{exp}, and the simulated neutron sensitivity with two neutron libraries: ENDF/B-VII.0 and JEFF-3.1.

$\overline{E}_n$ (keV)	Signal range (MeV)	N_c	ϵ_n^{exp} (%)	ϵ_n^{ENDFB} (%)	ϵ_n^{JEFF} (%)
42	1.6–8	$1.304(11)\times10^4$	1.76(4)	0.78	1.01
128	1.6–8	$1.169(11)\times10^4$	0.37(1)	0.42	0.58
507	0.05–0.55	$7.87(16)\times10^4$	3.44(15)	3.13	2.12
1031	0.05–1.1	$2.39(5)\times10^5$	5.28(13)	5.17	3.88
2242	0.05–2.6	$6.37(6)\times10^5$	7.2(7)	7.39	6.31

4.1. Comparison with experimental results

The simulations were carried out using release 9.4 (patch 01) of the Geant4 simulation toolkit. The associated neutron data library is the G4NDL-3.14 version. This version is based on release VI.8 of ENDF/B with a number of additions from other databases. For verification the simulations were repeated with a newer release (9.6, patch 03) of Geant4. The associated neutron data library is G4NDL-4.2, which is based on version VII.1 of ENDF/B. At the end of this section there is a brief comment on the results obtained with the new Geant4 release.

In the simulations we use the geometrical description of the $LaBr_3$:Ce crystal module provided by the manufacturer (see Section 3). We assume a standard 5% Ce doping concentration. Variations of the concentration up to 10% do not have a significant impact on the simulations. As for the unknown composition of the reflector and damping materials, after several tests which show little sensitivity, we fix it to be a single layer of silicone putty with standard composition. Neither the PMT nor the supporting structure is included in the simulation. Neutrons are emitted in a narrow cone subtending the crystal capsule from a distance of 1 m. The energy of the neutron is sampled from the measured neutron energy distribution. A total of 10 million events are simulated for each run. All the simulations are convoluted with the measured instrumental resolution function (Section 3.2).

MC simulations of the detector response were performed for all five measured quasi-monoenergetic neutron beams using the Geant4 distributed G4NDL-3.14 library as well as the standard libraries ENDF/B-VI.8, ENDF/B-VII.0, JEFF-3.1 and JENDL-3.3. As explained in Ref. [20], few Geant4 classes need to be updated in order to use the latter with release 9.4. When they are compared, the results of the simulations using the different libraries can be clearly separated into two groups. In each group, independent of the neutron energy, the results are very similar (although not exactly identical) and different from the other group. As an example we show in Fig. 5 the comparison of the five libraries for the distribution with average neutron energy $\overline{E}_n = 1031$ keV. As can be observed the results of ENDF/B-VII.0 and JENDL-3.3 are very similar (except for the first peak at 166 keV not easily distinguishable in the figure) while the results of G4NDL-3.14, ENDF/B-VI.8 and JEFF-3.1 are also very similar to each other (except for the peak at 166 keV and above 600 keV) and differ from the first two. Initial simulations included also the JENDL-4.0 library. However it produces such a poor reproduction of the measured spectra that it was not further included in the comparison.

The comparison with the experimental response is shown in Fig. 6. For clarity in this figure (and in subsequent figures) we only show the simulation results with the ENDF/B-VII.0 and JEFF-3.1 libraries since they are representative of the results of the two groups. A remarkable agreement is found between the experimental results and the simulation using the ENDF/B-VII.0 database. The simulation with JEFF-3.1 reproduces the peaks observed up to 530 keV but largely under-predicts the number of γ-rays above this energy. This also explains the smaller height of the

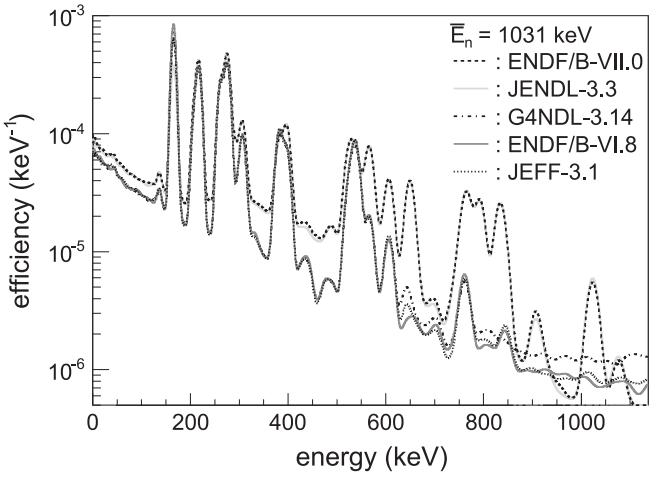

Fig. 5. MC simulated detector response using five different neutron libraries for the distribution with $\overline{E}_n = 1031$ keV.

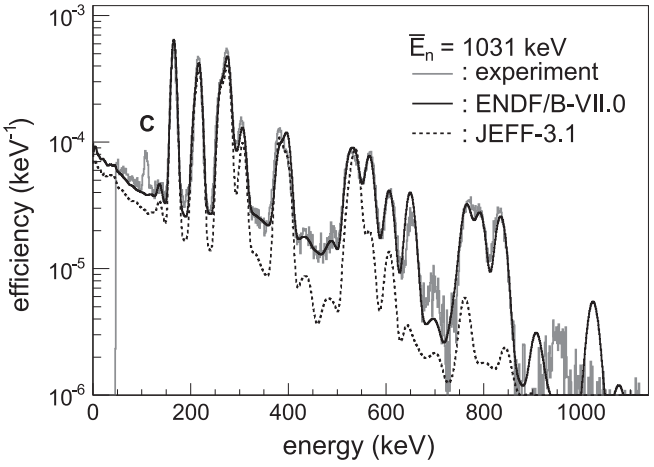

Fig. 6. Comparison of measured and simulated detector response with two different neutron libraries for the distribution with $\overline{E}_n = 1031$ keV. C: contaminant peak.

continuum at lower energies which is due to Compton interactions. It should be noted that no additional normalization has been introduced in this comparison. All the peaks observed up to 900 keV can be identified as coming from the de-excitation of levels populated in the inelastic scattering of the most abundant isotopes in the crystal (^{79,81}Br, ^{139}La). The exception is the peak marked with C which we believe corresponds to the ^{19}F 110 keV γ-ray. MC simulations have shown that such peak could be produced by neutron inelastic scattering if Teflon is used as a reflecting material in the detector.

Fig. 7 shows the comparison of measured and simulated response for the neutron beam with $\overline{E}_n = 2242$ keV. As can be observed the reproduction of the experimental spectrum is quite good up to about 1.3 MeV when the ENDF/B-VII.0 database is used in the simulation. Above this energy the discrepancies become larger. In the case of the JEFF-3.1 library the agreement is not satisfactory above 400 keV. This is due to the fact that in general the calculated intensity of the transitions is smaller or even zero when this database is used. The contaminant peak at 110 keV is again visible in the experimental spectrum.

The comparison for the neutron distribution with average energy $\overline{E}_n = 507$ keV is shown in Fig. 8. Here again the ENDF/B-VII.0 simulated response gives a better reproduction of the experimental results than the simulated response with JEFF-3.1.

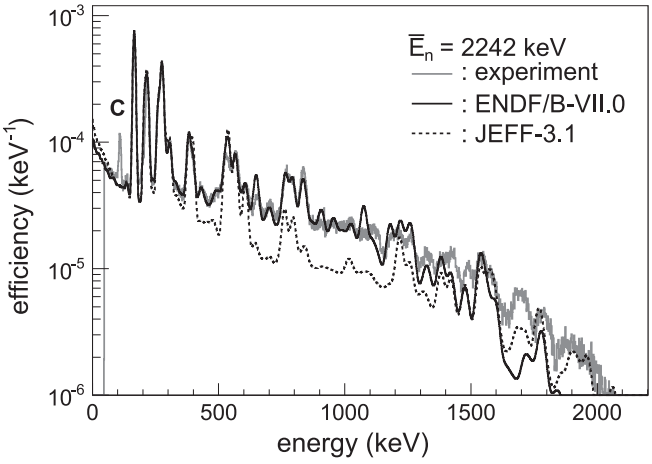

Fig. 7. Same as Fig. 6 for $\overline{E}_n = 2242$ keV.

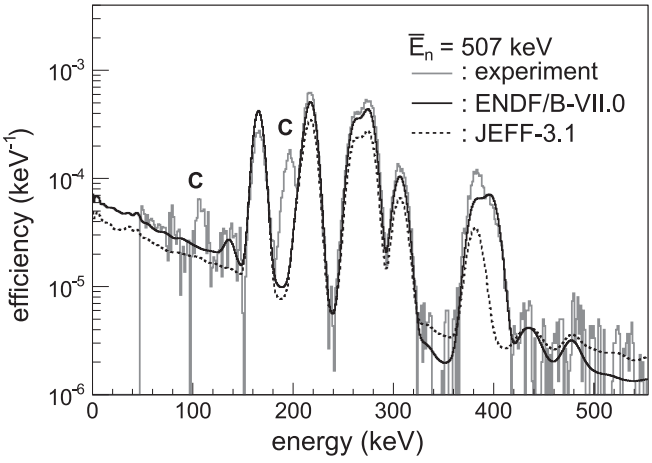

Fig. 8. Same as Fig. 6 for $\overline{E}_n = 507$ keV.

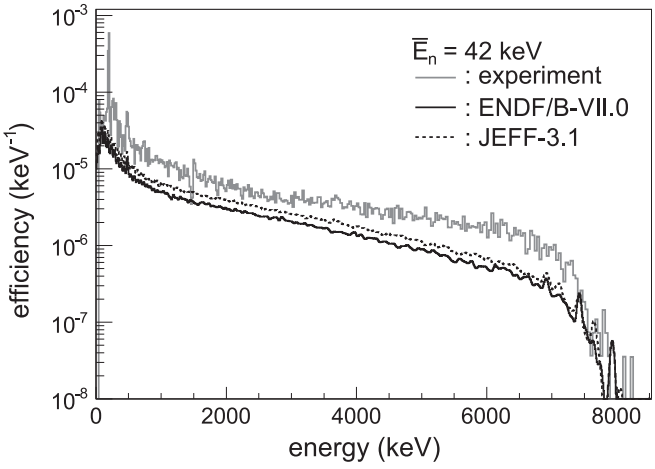

Fig. 9. Same as Fig. 6 for $\overline{E}_n = 42$ keV. The background (visible below 1.6 MeV) was not subtracted in this case.

In the experimental distribution, apart from the 110 keV peak, an additional strong contaminant peak can be observed at 197 keV. We identify both peaks as coming from the de-excitation of ^{19}F.

The detector response at the three neutron beam energies discussed above is dominated by the inelastic scattering process. At $\overline{E}_n = 42$ keV only the capture channel is open. The comparison of the measured response with the simulated one is shown in Fig. 9. In this case, as mentioned above, no background subtraction was

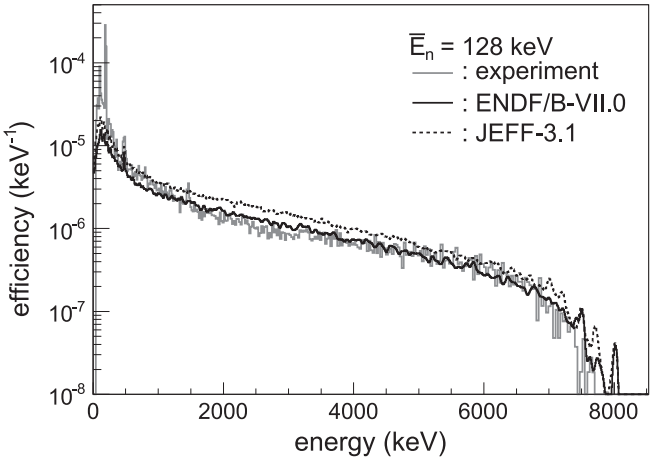

Fig. 10. Same as Fig. 9 for $\overline{E}_n = 128$ keV.

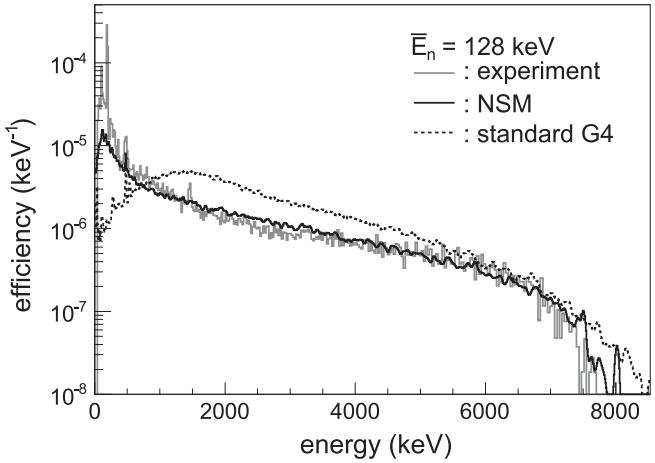

Fig. 11. Comparison of measured and simulated detector response with ENDF/B-VII.0 neutron library using the standard Geant4 capture cascade generator and the NSM cascade generator for $\overline{E}_n = 128$ keV.

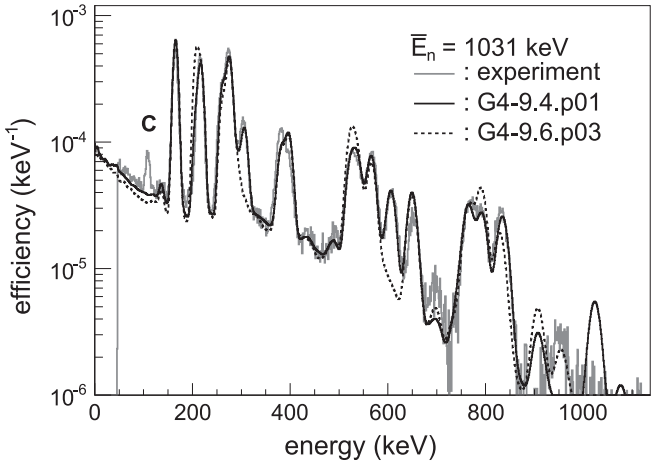

Fig. 12. Comparison of measured and simulated detector response with the ENDF/B-VII.0 neutron library using two different Geant4 releases for $\overline{E}_n = 1031$ keV.

performed and one can see in the spectrum the contaminant peaks at 110 keV, 197 keV, 478 keV and the group at 1436–1460 keV. However the background contribution is negligible above 1.6 MeV. As can be observed the spectrum extends up to 8 MeV showing the effect of the high energy electromagnetic cascades. The MC simulated responses although reproducing fairly well the shape of the spectrum fail to reproduce the height by a factor two or three. The result obtained with JEFF-3.1 is about 30% larger (integrated value) than the one obtained with ENDF/B-VII.0.

The measurement with average neutron energy $\overline{E}_n = 128$ keV is also dominated by capture reactions and the spectrum is shown in Fig. 10. Similar to the previous case no background subtraction was performed and the contaminant peaks are visible in the spectrum. Simulations performed with the two libraries are also shown in Fig. 10. A fairly good agreement, in shape and magnitude, is obtained between the simulation using ENDF/B-VII.0 and the measurement. The result obtained with JEFF-3.1 is, on average, about 40% larger.

All the simulations shown above made use of the NSM capture cascade generator. At this point it is relevant to show the effect of using the standard Geant4 cascade generator instead. This is done in Fig. 11 where we compare the results of both cascade generators using the ENDF/B-VII.0 library in the case of $\overline{E}_n = 128$ keV. As can be observed the spectrum produced by the standard generator does not reproduce the shape of the experimental spectrum and shows a maximum around 1.4 MeV. A similar picture is obtained at $\overline{E}_n = 42$ keV. The superior performance of the NSM generator is clear in the simulation of the response of detectors to low energy neutrons where the interaction is dominated by radiative capture.

The simulated neutron sensitivity is calculated for both the ENDF/B-VII.0 and JEFF-3.1 libraries and is compared with the experimental value in Table 3. A quite good agreement is observed between the measurement and the simulation when the ENDF/B-VII.0 library is used at all energies except the lowest. The values obtained with JEFF-3.1 are consistently lower at the energies dominated by the inelastic process and higher for those where the capture channel is the only open one.

As mentioned at the beginning of this section the simulations were repeated with a newer release (9.6.p03) of Geant4. The first observation is that the results obtained with the accompanying standard library G4NDL-4.2, based on release VII.1 of the ENDF/B neutron data library, are practically indistinguishable from those obtained with ENDF/B-VII.0. When compared to the simulations reported previously in this section, obtained with the 9.4.p01 release, using the same neutron data library we find small but significant differences. We show in Fig. 12 the comparison of the simulations carried out with the ENDF/B-VII.0 library for the distribution with average neutron energy $\overline{E}_n = 1031$ keV. As can be observed, the height of some of the peaks in both simulations is quite different. The same behavior is observed at $\overline{E}_n = 507$ keV and $\overline{E}_n = 2242$ keV and for the other neutron data libraries. Overall there is a deterioration in the agreement with experiment for the simulations performed with the newer release. This is an unexpected result considering that we are using the same cross-section and inelastic γ-ray files. We are currently investigating the origin of these differences.

5. Summary and conclusions

The neutron sensitivity of a ⊘ 1.5 in. × 1.5 in. $LaBr_3$:Ce detector was measured using quasi-monoenergetic neutron beams at five different energies in the range from 40 keV to 2.5 MeV. The ability to reproduce the measured response using the Geant4 simulation toolkit was investigated. For this we used a new tool that allows one to perform simulations with standard neutron data libraries in addition to G4NDL, the library supplied in Geant4. In addition, a generator of capture γ-ray cascades was implemented to replace the standard Geant4 generator, which uses the information in the nuclear databases which is often incomplete. The new generator is based on the statistical model of the nucleus and should be able to

describe realistically the multiplicity and energy distribution of capture cascades.

It was found that a remarkable good reproduction of the position and height of the γ-ray peaks associated with the neutron inelastic scattering process, dominant at 507, 1031 and 2242 keV average neutron energies, could be obtained for the ENDF/B-VII.0 or the JENDL-3.3 libraries when release 9.4.p01 of Geant4 is used. The agreement is much worse when we use instead the G4NDL-3.14, ENDF/B-VI.8 or JEFF-3.1 libraries. At neutron energies below the inelastic threshold in $LaBr_3$:Ce, 42 keV and 128 keV, the response is due to neutron capture processes in the detector. The first conclusion that can be drawn is that in order to reproduce the shape of the response it is necessary to use the new nuclear statistical model cascade generator. The standard generator fails to reproduce the shape. Concerning the magnitude, we find a difference for the two energies. While a good agreement is found at 128 keV when the ENDF/B-VII.0 or the JENDL-3.3 libraries are used, the simulation underpredicts the value at 42 keV by more than a factor 2. In both cases the result with G4NDL-3.14, ENDF/B-VI.8 or JEFF-3.1 is about 40% larger than that obtained with the other libraries. At the energies where the inelastic channel dominates we find that simulations performed with the newer Geant4 9.6.p03 release differ from the previous ones and are poorer in terms of reproducing the spectra.

We conclude that the Geant4 simulation package with the flexibility provided by the new tool to incorporate standard neutron data libraries and the improved capture cascade generator is a useful tool to calculate scintillation detector responses to low energy neutrons. However we should warn the potential user that the quality of the reproduction of the measured data found in this paper should not be expected to hold necessarily for other setups. This depends on the quality of the information available in nuclear data libraries for the relevant isotopes and should be investigated in each case with test measurements.

Acknowledgments

This work has been supported by the Spanish Ministerio de Economía y Competitividad under Grants FPA2008-06419, FPA2010-17142 and FPA2011-24553, and CPAN CSD-2007-00042 (Ingenio2010), by the United States National Science Foundation under Grant no. PHY-1068192, and by EFNUDAT transnational access programme. H.M. acknowledges support from Grupo de Física Nuclear (Universidad Complutense) and from Instituto de Física Corpuscular (CSIC) during his stay as CPAN expert.

References

[1] E.V.D. van Loef, et al., Nuclear Instruments and Methods in Physics Research Section A 486 (2002) 254.
[2] B. Rubio, et al., Journal of Physics G 31 (2005) 1477.
[3] ⟨http://www.fair-center.eu/for-users/experiments/nustar/experiments/hispec despec.html⟩.
[4] D.E. Cullen, PREPRO 2007: 2007 ENDF/B Pre-Processing Codes, Report IAEA-NDS-39, Rev. 13, March 17, 2007.
[5] M.B. Chadwick, et al., Nuclear Data Sheets 107 (2006) 2931.
[6] R. Nicolini, et al., Nuclear Instruments and Methods in Physics Research Section A 582 (2007) 554.
[7] I. Bavykina, et al., Astroparticle Physics 28 (2007) 489.
[8] C. Guerrero, et al., Nuclear Instruments and Methods in Physics Research Section A 608 (2009) 424.
[9] Saint Gobain Crystals Home Page, ⟨http://www.crystals.saint-gobain.com/⟩.
[10] H.J. Brede, et al., Nuclear Instruments and Methods in Physics Research 169 (1980) 349.
[11] G. Lövestam, EnergySet: A Programme to Calculate Accelerator Settings and Neutron Yield Data for the IRMM VdG Laboratory, IRMM Internal Report GE/NP/2/2002/06/20, 2002.
[12] J. Agramunt, Desarrollo de un sistema de adquisicion de datos para fisica nuclear, Dissertation, University of Valencia, unpublished, July, 2002.
[13] J. De Pangher, L.L. Nichols, A Precision Long Counter for Measuring Fast Neutron Flux Density, Pacific Northwest Laboratory Report BNWL-260, 1966.
[14] R. Brun, F. Rademakers, Nuclear Instruments and Methods in Physics Research Section A 389 (1997) 81.
[15] S. Agostinelli, et al., Nuclear Instruments and Methods in Physics Research Section A 506 (2003) 250.
[16] K. Shibata, et al., Journal of Nuclear Science and Technology 39 (2002) 1125.
[17] A.J. Koning, et al., Journal of the Korean Physical Society 59 (2011) 1057.
[18] A.I. Blokhin, et al., Report IAEA-NDS-90 Rev. 8, Vienna, 1994.
[19] Z.G. Ge, et al., Journal of the Korean Physical Society 59 (2011) 1052.
[20] E. Mendoza, et al., IAEA Technical Report INDC(NDS)-0612, Vienna, 2012. Data Available online at ⟨http://www-nds.iaea.org/geant4. IEEE Transactions on Nuclear Science 61 (2014) 2357.
[21] J.L. Tain, D. Cano-Ott, Nuclear Instruments and Methods in Physics Research Section A 571 (2007) 719.